**Alien Earths** is part of NASA's Nexus for Exoplanetary System Science program, which carries out coordinated research toward the goal of searching for and determining the frequency of habitable extrasolar planets with atmospheric biosignatures in the Solar neighborhood.

Our interdisciplinary teams includes astrophysicists, planetary scientists, cosmochemists, material scientists, chemists, biologists, and physicists.

The Principal Investigator of Alien Earths is Daniel Apai (University of Arizona). The projects' lead institutions are The University of Arizona's Steward Observatory and Lunar and Planetary Laboratory.

For a complete list of publications, please visit the **AE Library** on the SAO/NASA Astrophysics Data System.

## Recent Publications

*Axisymmetric High Spot Coverage on Exoplanet Host HD 189733 A*

*Super-Earths and Earth-like Exoplanets*

*Repelling Planet pairs by Ping-pong Scattering*

*Differences between Stable and Unstable Architectures of Compact Planetary Systems*

*Where Are the Water Worlds? Identifying Exo-water-worlds Using Models of Planet Formation and Atmospheric Evolution*

*Petrogenesis of Erg Chech 002 Achondrite and Implications for an Altered Magma Ocean*

*JWST/NIRCam Imaging of Young Stellar Objects. I. Constraints on Planets Exterior to the Spiral Disk Around MWC 758*

*Distinguishing Oceans of Water from Magma on Mini-Neptune K2-18b*

*Statistical Distribution Function of Orbital Spacings in Planetary Systems*

*Bioverse: The Habitable Zone Inner Edge Discontinuity as an Imprint of Runaway Greenhouse Climates on Exoplanet Demographics*

*Empirically Constraining the Spectra of Stellar Surface Features Using Time-resolved Spectroscopy*

*HST astrometry of the closest brown dwarfs-II. Improved parameters and constraints on a third body*

# *ALIEN EARTHS ALL HANDS MEETING 2024*

## Hacienda Del Sol | April 23-25th

# *ALIEN EARTHS ALL HANDS MEETING 2024*

## Hacienda Del Sol | April 23-25th


# *Axisymmetric High Spot Coverage on Exoplanet Host HD 189733 A*

Isaac S. Narrett, Benjamin V. Rackham, and Julien de Wit

The Astronomical Journal, Volume 167, Issue 3

Transmission spectroscopy is a powerful tool to study exoplanet atmospheres, which can be affected by the ability of stellar photospheric heterogeneity to mimic or mask exoplanetary spectral signatures. The canonical HD 189733 system provides a textbook example of this spectroscopic discrepancy with features that have been variously interpreted as signatures of scattering by haze in the planetary atmosphere or unocculted spots on the stellar disk. Here, we leverage three archival data sets from the Hubble Space Telescope to directly infer the covering fraction of HD 189733 A and explore the evidence for photospheric heterogeneity in the out-of-transit spectra. We model the stellar spectrum using one to three spectral components in a nested-sampling framework, finding that the two-component model (photosphere and spot) is preferred for all data sets. We find photospheric and spot temperatures of ~5300 K and ~3200 K, respectively, which are consistent across data sets. The spot covering fraction is large and varies between 38% ± 4% and 47% ± 3%. Combined with time-domain insights from Transiting Exoplanet Survey Satellite data revealing HD 189733 A's 1.4% peak-to-peak variability, our findings imply that most of the spots must be distributed axisymmetrically, e.g., in a densely filled latitudinal band or at the poles. More work with complementary data sets is necessary to investigate those possible arrangements.

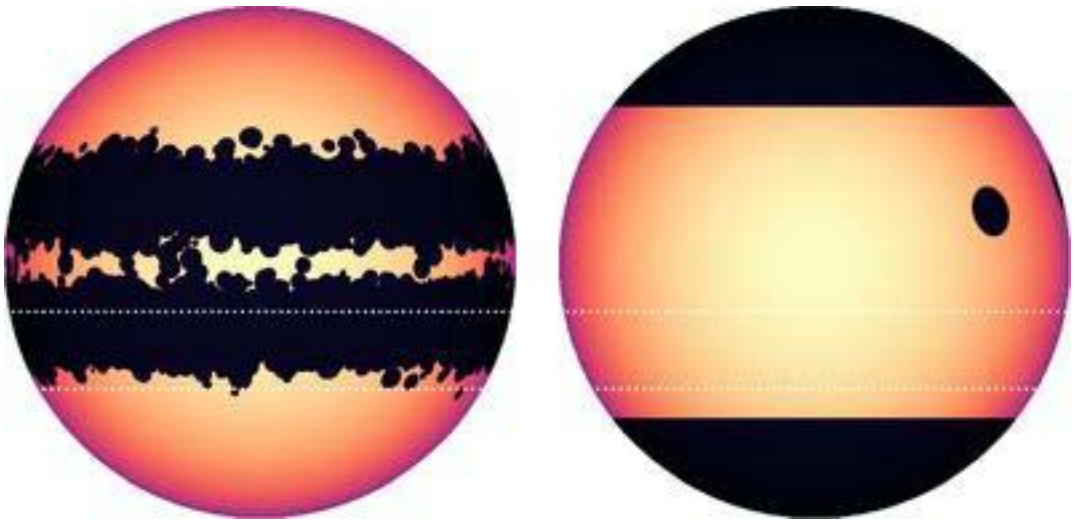

**Figure 7.** Examples of hypothetical spot distributions with ~40% spot coverage and ~1.4% rotational variability in the TESS bandpass. The left panel provides an example of densely filled latitudinal spot bands in which overdensities of spots lead to rotational variability and apparent spot-crossing events, while the right shows large, nonvariable polar spots with a few additional spots that produce the variability and occasional spot-crossing event. The region occulted by HD 189733 b is outlined by dotted white lines in both panels. Made with spotter (Garcia & Rackham) **2023).**

# *Super-Earths and Earth-like Exoplanets*

Tim Lichtenberg, Yamila Miguel

Treatise on Geochemistry, 3rd edition

In the last few years astronomical surveys have expanded the reach of planetary science into the realm of small and dense extrasolar worlds. These share a number of characteristics with the terrestrial and icy planetary objects of the Solar System, but keep stretching previous understanding of the known limits of planetary thermodynamics, material properties, and climate regimes. Improved compositional and thermal constraints on exoplanets below ~2 Earth radii suggest efficient accretion of atmosphere-forming volatile elements in a fraction of planetary systems, pointing to rapid formation, planet-scale melting, and chemical equilibration between the core, mantle, and atmosphere of rocky and volatile-rich exoplanets. Meaningful interpretation of novel observational data from these worlds necessitates cross-disciplinary expansion of known material properties under extreme thermodynamic, non-solar conditions, and accounting for dynamic feedbacks between interior and atmospheric processes. Exploration of the atmosphere and surface composition of individual, short-period super-Earths in the next few years will enable key inferences on magma ocean dynamics, the redox state of rocky planetary mantles, and mixing between volatile and refractory phases in planetary regimes that are absent from the present-day Solar System, and reminiscent of the conditions of the prebiotic Earth. The atmospheric characterization of climate diversity and the statistical search for biosignatures on terrestrial exoplanets on temperate orbits will require space-based direct imaging surveys, capable of resolving emission features of major and trace gases in both shortwave and mid-infrared wavelen

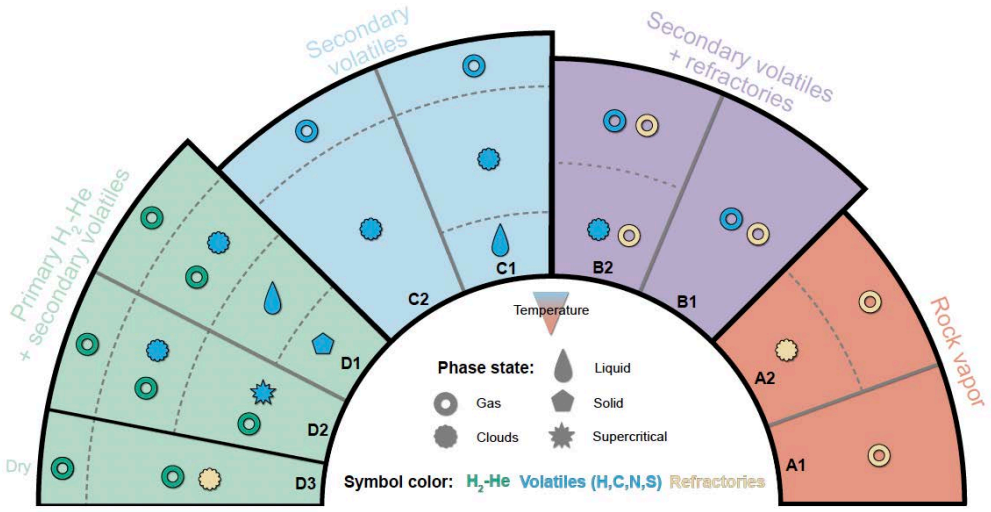


**Figure 6.** Illustration of plausible classes of atmospheres on super-Earths and Earth-like exoplanets expected from theoretical calculations and observational constraints. The different radii in each case represent the increase in mean molecular weight expected from H- (left) to rock-dominated (right). Different symbols show the presence of gases or condensates in the atmospheres. Information on liquids, solids or supercritical fluid at higher pressures is also shown. Temperatue generally increases from top (blue, purple) to bottom (green, red) classes, either driven by stellar irradiation (red) or greenhouse forcing (green). Note that the separation in different layers is schematic and does not represent the actual depth of such layers in the planet.

# *Repelling Planet pairs by Ping-pong Scattering*

Yanqin Wu , Renu Malhotra, Yoram Lithwick

Submitted to: AAS Journal

The Kepler mission reveals a peculiar trough-peak feature in the orbital spacing of close-in planets near mean-motion resonances: a deficit and an excess that are a couple percent to the narrow, respectively wide, of the resonances. This feature has received two main classes of explanations, one involving eccentricity damping, the other scattering with small bodies. Here, we point out a few issues with the damping scenario, and study the scattering scenario in more detail. We elucidate why scattering small bodies tends to repel two planets. As the small bodies random-walk in energy and angular momentum space, they tend to absorb, fractionally, more energy than angular momentum. This, which we call "ping-pong repulsion", transports angular momentum from the inner to the outer planet and pushes the two planets apart. Such a process, even if ubiquitous, leaves identifiable marks only near first-order resonances: diverging pairs jump across the resonance quickly and produce the MMR asymmetry. To explain the observed positions of the trough-peaks, a total scattering mass of order a few percent of the planet masses is required. Moreover, if this mass is dominated by a handful of Mercury-sized bodies, one can also explain the planet eccentricities as inferred from transit-time-variations. Lastly, we suggest how these conditions may have naturally arisen during the late stages of planet formation.

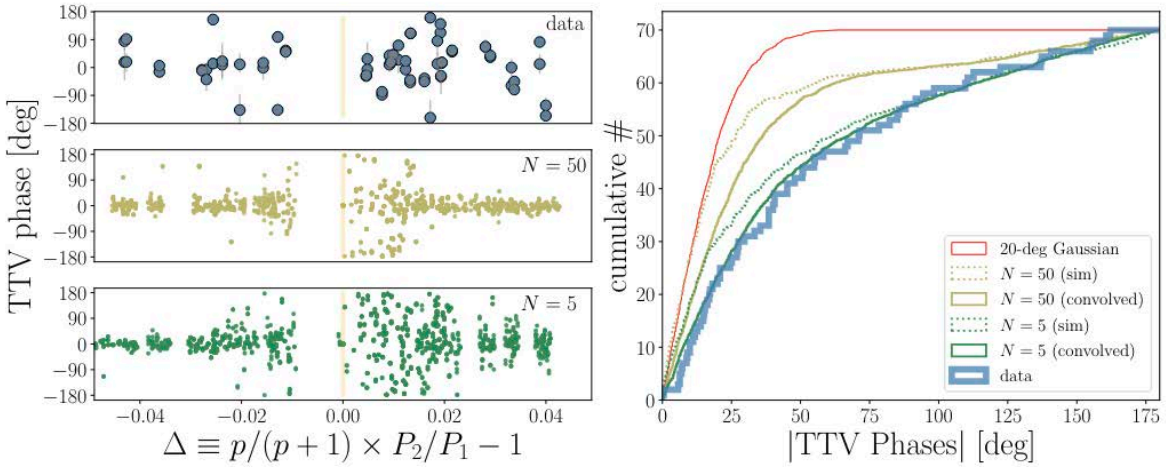


**Figure 11.** Comparing TTV phases between data and simulations. For the observed values, we take the same 35 pairs from Fig. 2 and express their period ratios as $\Delta = p/(p+1)\ P_2/P_1 - 1$ to capture their respective MMRs. The simulations are the two sets from Fig. 9. The left panels compare how the TTV phase depend on the distance to the MMR, and the right compares the cumulative distributions of the TTV phases. Here, the red curve describes a population with zero free-eccentricities (convolved with the typical noise, a Gaussian of 20 deg), and represents the prediction from repulsion by e-damping. The simulation with heavy ping-pongs, after convolving with the same Gaussian, agrees well with the observed TTV phase distributions (p-value 0.9). The lighter ping-pong model, on the other hand, has a p-value of 0.0015. This suggests that individual planetesimals should have ~ Mercury mass.

# *Differences between Stable and Unstable Architectures of Compact Planetary Systems*

Kathryn Volk and Renu Malhotra

The Astronomical Journal, Volume 167, Issue 6

We present a stability analysis of a large set of simulated planetary systems of three or more planets based on architectures of multiplanet systems discovered by Kepler and K2. We propagated 21,400 simulated planetary systems up to 5 billion orbits of the innermost planet; approximately 13% of these simulations ended in a planet–planet collision within that time span. We examined trends in dynamical stability based on dynamical spacings, orbital period ratios, and mass ratios of nearest-neighbor planets as well as the system-wide planet mass distribution and the spectral fraction describing the system's short-term evolution. We find that instability is more likely in planetary systems with adjacent planet pairs that have period ratios less than 2 and in systems of greater variance of planet masses. Systems with planet pairs at very small dynamical spacings (less than ~10–12 mutual Hill radii) are also prone to instabilities, but instabilities also occur at much larger planetary separations. We find that a large spectral fraction (calculated from short integrations) is a reasonable predictor of longer-term dynamical instability; systems that have a large number of Fourier components in their eccentricity vectors are prone to secular chaos and subsequent eccentricity growth and instabilities.

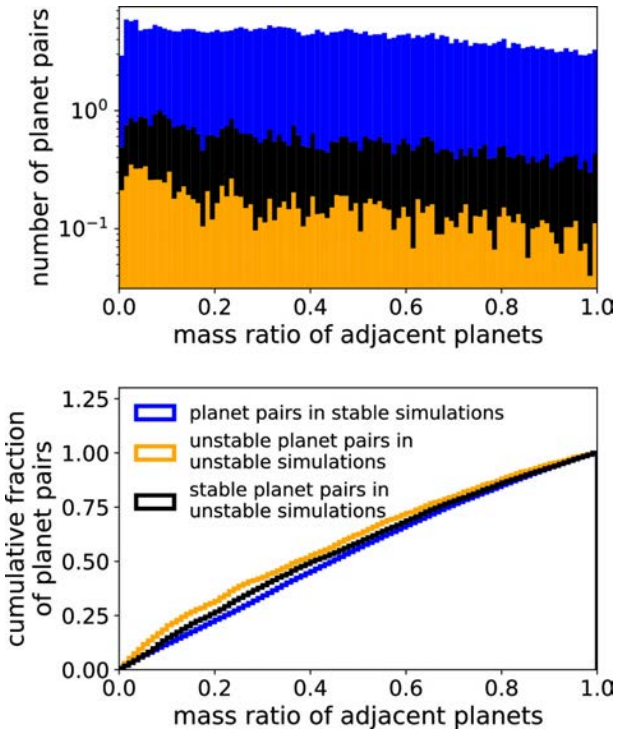


**Figure 10.** All simulations: distribution of mass ratios between neighboring planets (top: stacked histogram weighted to the observed number of planet pairs; bottom: normalized cumulative distributions). Note the log scale in the top panel used to better highlight the distribution of the colliding pairs. Colliding planet pairs are shown in orange with the other adjacent planet pairs in those simulations shown in black. Planet pairs in simulations with no collisions are shown in blue. Note that a few percent of the colliding pairs of planets were not adjacent at the start of the simulations.

# *Where Are the Water Worlds? Identifying Exo-water-worlds Using Models of Planet Formation and Atmospheric Evolution*

Aritra Chakrabarty and Gijs D. Mulders

The Astrophysical Journal, Volume 966, Number 2

Planet formation models suggest that the small exoplanets that migrate from beyond the snowline of the protoplanetary disk likely contain water-ice-rich cores (~50% by mass), also known as water worlds. While the observed radius valley of the Kepler planets is well explained by the atmospheric dichotomy of the rocky planets, precise measurements of the mass and radius of the transiting planets hint at the existence of these water worlds. However, observations cannot confirm the core compositions of those planets, owing to the degeneracy between the density of a bare water-ice-rich planet and the bulk density of a rocky planet with a thin atmosphere. We combine different formation models from the Genesis library with atmospheric escape models, such as photoevaporation and impact stripping, to simulate planetary systems consistent with the observed radius valley. We then explore the possibility of water worlds being present in the currently observed sample by comparing them with simulated planets in the mass–radius–orbital period space. We find that the migration models suggest ≳10% and ≳20% of the bare planets, i.e., planets without primordial H/He atmospheres, to be water-ice-rich around G- and M-type host stars, respectively, consistent with the mass–radius distributions of the observed planets. However, most of the water worlds are predicted to be outside a period of 10 days. A unique identification of water worlds through radial velocity and transmission spectroscopy is likely to be more successful when targeting such planets with longer orbital periods.

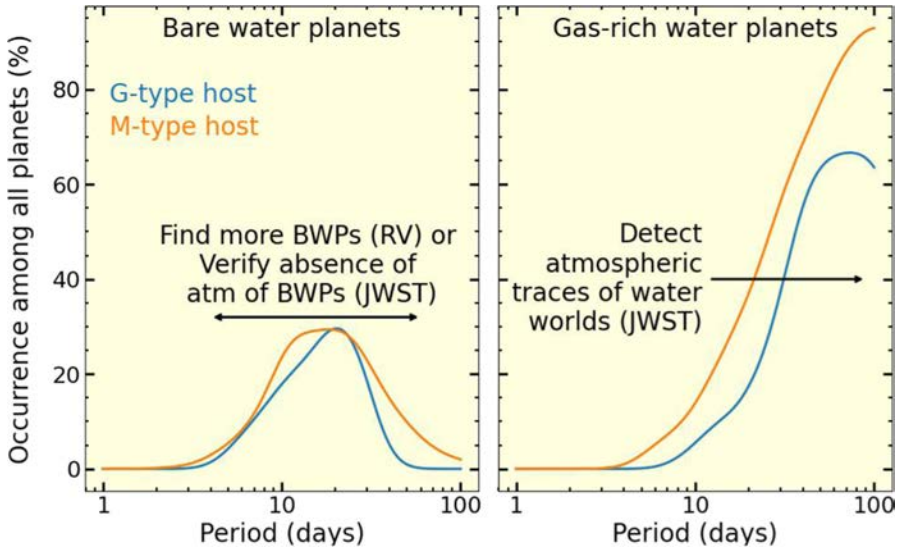


**Figure 12.** Fractional occurrence of water worlds as functions of the orbital period predicted by our migration + photoevaporation model for the G-type host star. While the BWPs and GWPs are likely to be concentrated beyond orbital periods of 10 days, it is more likely to find a water planet around an M dwarf than around a G dwarf.

# *Petrogenesis of Erg Chech 002 Achondrite and Implications for an Altered Magma Ocean*

Ziliang Jin, Yishen Zhang, Maitrayee Bose, Sarah Glynn, and Frédéric Couffignal

The Astrophysical Journal, Volume 965, Issue 1

This study conducts mineralogical and chemical investigations on the oldest achondrite, Erg Chech 002 (~4565 million yr old). This meteorite exhibits a disequilibrium igneous texture characterized by high-Mg-number (atomic Mg/(Mg + Fe2+)) orthopyroxene xenocrysts (Mg number = 60–80) embedded in an andesitic groundmass. Our research reveals that these xenocrysts were early formed crystals, loosely accumulated or scattered in the short-period magma ocean on the parent body. Subsequently, these crystals underwent agitation due to the influx of external materials. The assimilation of these materials enriched the 16O component of the magma ocean and induced a relatively reduced state. Furthermore, this process significantly cooled the magma ocean and inhibited the evaporation of alkali elements, leading to elevated concentrations of Na and K within the meteorite. Our findings suggest that the introduced materials are probably sourced from the reservoirs of CR clan meteorites, indicating extensive transport and mixing of materials within the early solar system.

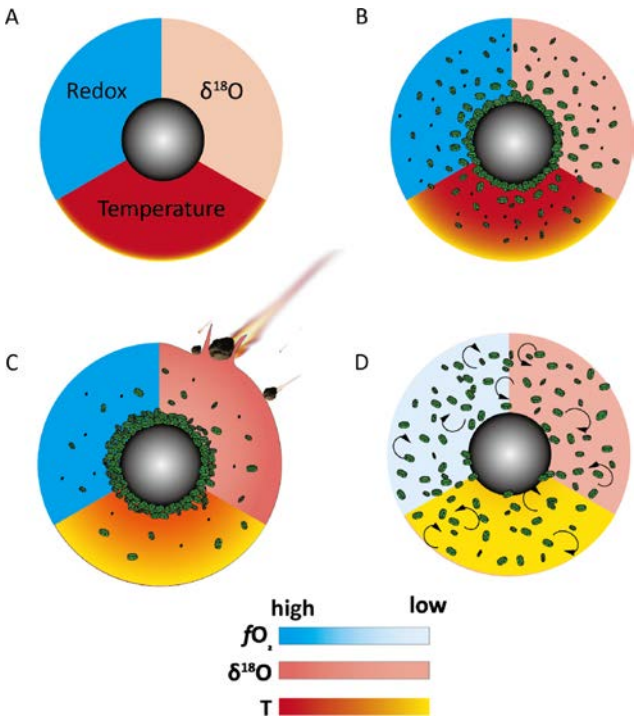


**Figure 7.** A schematic showing the evolutional history of EC 002 parent body. The whole process is divided into four stages. (A) Initial differentiation of the parent body led to core–mantle segregation and the establishment of a hot and oxidized magma ocean. (B) During the second stage, high-Mg Opx crystallized and loosely accumulated or scattered within the magma ocean. (C) The addition of external materials not only induced cooling and chemical or isotopic alterations in the magma ocean but also disturbed the early formed high-Mg Opx. (D) Eventually, the evenly distributed high-Mg Opx occurs as xenocrysts after the solidification of the parent body.

# *JWST/NIRCam Imaging of Young Stellar Objects. I. Constraints on Planets Exterior to the Spiral Disk Around MWC 758*

Kevin Wagner et al 2024

The Astronomical Journal, Volume 167, Issue 4

MWC 758 is a young star hosting a spiral protoplanetary disk. The spirals are likely companion-driven, and two previously identified candidate companions have been identified—one at the end the Southern spiral arm at ~0.″6, and one interior to the gap at ~0.″1. With JWST/NIRCam, we provide new images of the disk and constraints on planets exterior to ~1″. We detect the two-armed spiral disk, a known background star, and a spatially resolved background galaxy, but no clear companions. The candidates that have been reported are at separations that are not probed by our data with sensitivity sufficient to detect them-nevertheless, these observations place new limits on companions down to ~2 M Jup at ~150 au and ~0.5 M Jup at ≳600 au. Owing to the unprecedented sensitivity of JWST and youth of the target, these are among the deepest mass-detection limits yet obtained through direct imaging observations, and provide new insights into the system's dynamical nature.

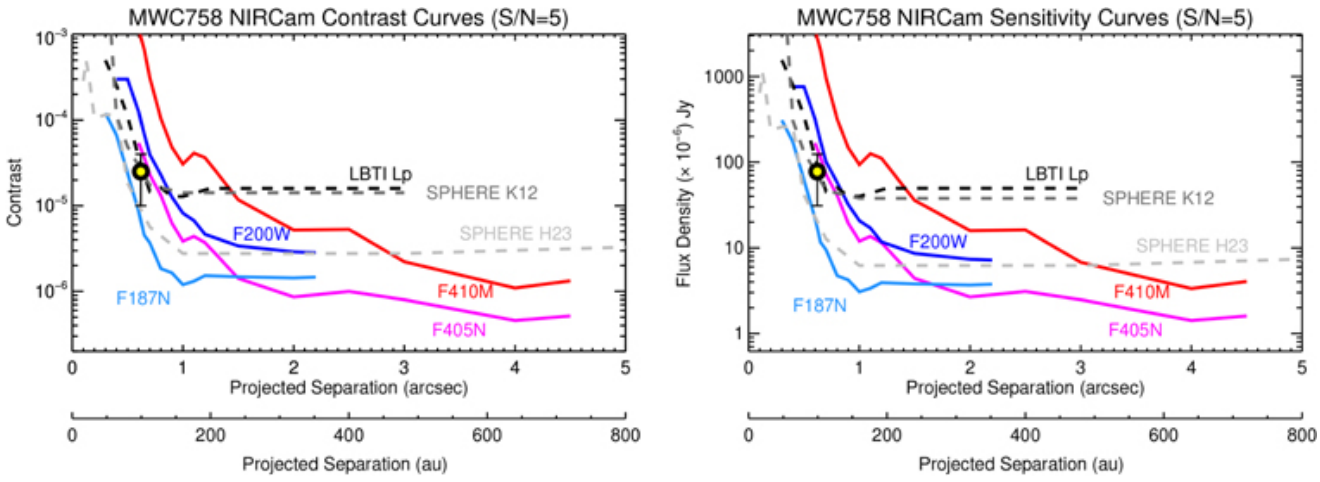


**Figure 3.** Contrast curves generated via synthetic point source injections. Comparisons to ground-based data (Wagner et al. 2019; Boccaletti et al. 2021) at similar wavelengths are shown in dashed curves. F187N is most comparable in wavelength to SPHERE's H23 filter, F200W is most comparable to SPHERE's K12 filter, and F405N and F410M are most comparable to LBTI's Lp (or *L′*) filter. The yellow circle corresponds the brightness of MWC 758 c measured at 4.05 μm with LBTI/ALES (Wagner et al. 2023). At wavelengths longer than λ ≳ 2 μm and projected separations ≳1", the NIRCam data reach over an order of magnitude fainter sensitivities than ground-based data. These sensitivities are converted to mass-detection limits in Figure 4. The scattered light disk extends to ~055 (Benisty et al. 2015). Sensitivities interior to this are likely underestimated as a result.

# *Distinguishing Oceans of Water from Magma on Mini-Neptune K2-18b*

Oliver Shorttle, Sean Jordan, Harrison Nicholls, Tim Lichtenberg, and Dan J. Bower

The Astrophysical Journal Letters, Volume 962, Issue 1

Mildly irradiated mini-Neptunes have densities potentially consistent with them hosting substantial liquid-water oceans ("Hycean" planets). The presence of CO2 and simultaneous absence of ammonia (NH3) in their atmospheres has been proposed as a fingerprint of such worlds. JWST observations of K2-18b, the archetypal Hycean, have found the presence of CO2 and the depletion of NH3 to <100 ppm; hence, it has been inferred that this planet may host liquid-water oceans. In contrast, climate modeling suggests that many of these mini-Neptunes, including K2-18b, may likely be too hot to host liquid water. We propose a solution to this discrepancy between observation and climate modeling by investigating the effect of a magma ocean on the atmospheric chemistry of mini-Neptunes. We demonstrate that atmospheric NH3 depletion is a natural consequence of the high solubility of nitrogen species in magma at reducing conditions; precisely the conditions prevailing where a thick hydrogen envelope is in communication with a molten planetary surface. The magma ocean model reproduces the present JWST spectrum of K2-18b to ≲3σ, suggesting this is as credible an explanation for current observations as the planet hosting a liquid-water ocean. Spectral areas that could be used to rule out the magma ocean model include the >4 μm region, where CO2 and CO features dominate: magma ocean models suggest a systematically lower CO2/CO ratio than estimated from free-chemistry retrieval, indicating that deeper observations of this spectral region may be able to distinguish between oceans of liquid water and magma on mini-Neptunes.

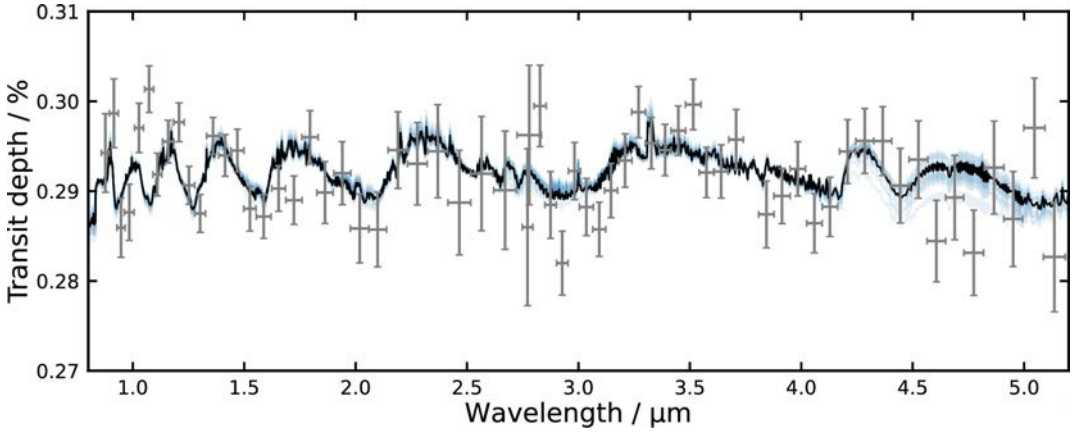


**Figure 4.** Best-fitting model transmission spectra of the atmospheres in the magma ocean scenario. The transmission spectra are generated, using petitRADTRANS, from the output photochemical-kinetics models when taking the atmosphere–magma ocean system output as a lower boundary condition (step 4, Figure 1). Data points from the observed transmission spectrum of K2-18b (Madhusudhan et al. 2023b) are plotted with their associated error estimates. The best-fitting model in the magma ocean scenario is shown in black and all models that agree with the observational data within 3σ are shown in blue.

# *Statistical Distribution Function of Orbital Spacings in Planetary Systems*

Jamie Dietrich, Renu Malhorta, Dániel Apai

The Astronomical Journal, Volume 167, Number 2

The minimum orbital separation of planets in long-stable planetary systems is often modeled as a step function, parameterized with a single value $\Delta_{min}$ (measured in mutual Hill radius of the two neighboring planets). Systems with smaller separations are considered unstable, and planet pairs with greater separations are considered stable. Here we report that a log-normal distribution function for $\Delta_{min}$, rather than a single threshold value, provides a more accurate model. From our suite of simulated planetary systems, the parameters of the best-fit log-normal distribution are $\mu = 1.97 \pm 0.02$ and $\sigma = 0.40 \pm 0.02$, such that the mean, median, and mode of $\Delta_{min}$ are 7.77, 7.17, and 6.11, respectively. This result is consistent with previous estimates for $\Delta_{min}$ threshold values in the range ~5–8. We find a modest dependence of the distribution of $\Delta_{min}$ on multiplicity within the system, as well as on planetary mass ratios of the closest planet pair. The overall distribution of nearest-neighbor planetary orbital spacings (measured in the mutual Hill radii and denoted simply as $\Delta$) in long-term stable systems is also well fit with a log-normal distribution, with parameters $\mu = 3.14 \pm 0.03$ and $\sigma = 0.76 \pm 0.02$. In simulations of sets of many planets initially packed very close together, we find that the orbital spacings of long-term stable systems is statistically similar to that in the observed Kepler sample of exoplanetary systems, indicating a strong role of sculpting of planetary architectures by dynamical instabilities.

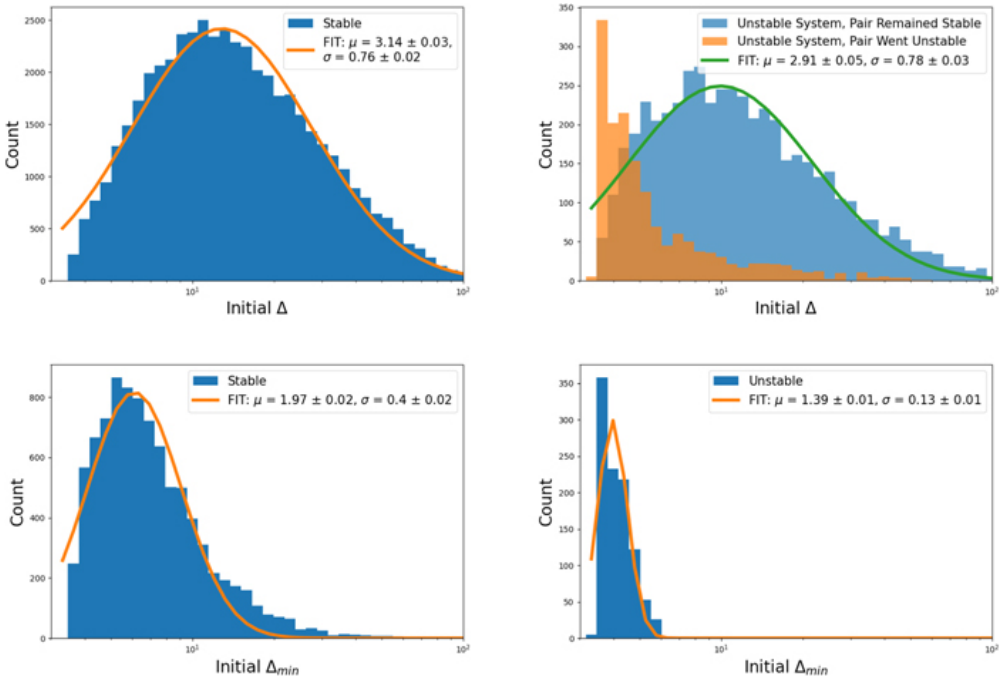


**Figure 3.** Results for the Nominal Kepler Analog Set. Top: histogram of all the $\Delta$ values for each nearest-neighbor planet pair in stable systems (left) and unstable systems (right). Bottom: histogram of the initial $\Delta_{min}$ distribution and the best-fit for log-normal function for stable systems (left) and unstable systems (right).

# *Bioverse: The Habitable Zone Inner Edge Discontinuity as an Imprint of Runaway Greenhouse Climates on Exoplanet Demographics*

Martin Schlecker, Dániel Apai, Tim Lichtenberg, Galen Bergsten, Arnaud Salvador and Kevin K. Hardegree-Ullman

The Planetary Science Journal, Volume 5, Issue 1

Long-term magma ocean phases on rocky exoplanets orbiting closer to their star than the runaway greenhouse threshold-the inner edge of the classical habitable zone-may offer insights into the physical and chemical processes that distinguish potentially habitable worlds from others. The thermal stratification of runaway planets is expected to significantly inflate their atmospheres, potentially providing observational access to the runaway greenhouse transition in the form of a habitable zone inner edge discontinuity in radius-density space. Here, we use Bioverse, a statistical framework combining contextual information from the overall planet population with a survey simulator, to assess the ability of ground- and space-based telescopes to test this hypothesis. We find that the demographic imprint of the runaway greenhouse transition is likely detectable with high-precision transit photometry for sample sizes ≳100 planets if at least ~10% of those orbiting closer than the habitable zone inner edge harbor runaway climates. Our survey simulations suggest that, in the near future, ESA's PLATO mission will be the most promising survey to probe the habitable zone inner edge discontinuity. We determine the survey strategies that maximize the diagnostic power of the obtained data and identify as key mission design drivers: (1) a follow-up campaign of planetary mass measurements and (2) the fraction of low-mass stars in the target sample. Observational constraints on the runaway greenhouse transition will provide crucial insights into the distribution of atmospheric volatiles among rocky exoplanets, which may help to identify the nearest potentially habitable worlds.

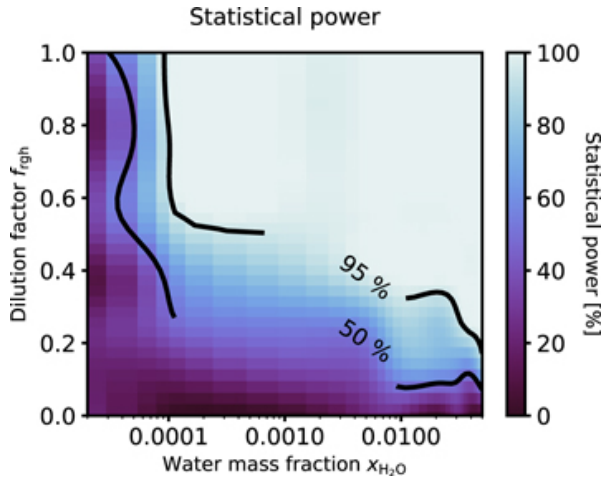


**Figure.** Figure 7. Statistical power of the runaway greenhouse hypothesis test as a function of model parameters. For a sample size N = 500, the color code shows the fraction of simulations resulting in a sound detection ($\Delta \ln \gtrsim > 3$) for different combinations of bulk water mass fraction and dilution factor. Higher values in either parameter result in a more reliable detection. For water mass fractions $\gtrsim 10^{-4}$, the statistical power largely depends on the

# *Empirically Constraining the Spectra of Stellar Surface Features Using Time-resolved Spectroscopy*

David Berardo, Julien de Wit, and Benjamin V. Rackham

The Astrophysical Journal Letters, Volume 961, Issue 1

Transmission spectroscopy is currently the technique best suited to study a wide range of planetary atmospheres, leveraging the filtering of a star's light by a planet's atmosphere rather than its own emission. However, as both a planet and its star contribute to the information encoded in a transmission spectrum, an accurate accounting of the stellar contribution is pivotal to enabling robust atmospheric studies. As current stellar models lack the required fidelity for such accounting, we investigate here the capability of time-resolved spectroscopy to yield high-fidelity, empirical constraints on the emission spectra of stellar surface heterogeneities (i.e., spots and faculae). Using TRAPPIST-1 as a test case, we simulate time-resolved JWST/NIRISS spectra and demonstrate that with a blind approach incorporating no physical priors, it is possible to constrain the photospheric spectrum to ≤0.5% and the spectra of stellar heterogeneities to within ≲10%, a precision that enables photon-limited (rather than model-limited) science. Now confident that time-resolved spectroscopy can propel the field in an era of robust high-precision transmission spectroscopy, we introduce a list of areas for future exploration to harness its full potential, including wavelength dependency of limb darkening and hybrid priors from stellar models as a means to further break the degeneracy between the position, size, and spectra of heterogeneities.

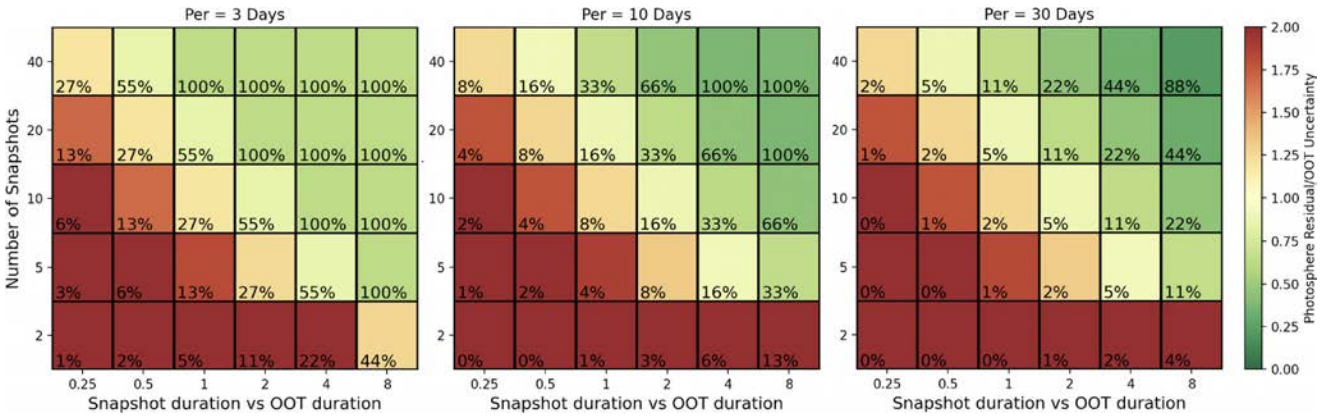


**Figure 4.** Long stare vs. series of snapshots, highlighting the effectiveness of different observing strategies for stars with rotation periods of 3, 10, and 30 days. Heat maps show the median residual on the photosphere spectrum when observing in snapshots (relative to the OOT uncertainty) for three different rotation periods. The percentage in each cell represents the total observation time relative to the rotation period of the star. The snapshot duration is relative to a 2 hr duration that would be typically observed OOT for a transit of planets around TRAPPIST-1.

# *HST astrometry of the closest brown dwarfs-II. Improved parameters and constraints on a third body*

L. R. Bedin, J. Dietrich, A. J. Burgasser, D. Apai, M. Libralato, M. Griggio, C. Fontanive, D. Pourbaix

Astronomische Nachrichten, Volume 345, Issue 1

Located at less than two pc away, Luhman 16 AB (WISE J104915.57-531906.1) is the closest pair of brown dwarfs and the third closest "stellar" system to Earth. An exoplanet candidate in the Luhman 16 binary system was reported in 2017 based on a weak astrometric signature in the analysis of 12 HST epochs. An additional epoch collected in 2018 and re-analysis of the data with more advanced methods further increased the significance level of the candidate, consistent with a Neptune-mass exoplanet orbiting one of the Luhman 16 brown dwarf components. We report the joint analysis of these previous data together with two new astrometric HST epochs we obtained to confirm or disprove this astrometric signature. Our new analysis rules out the presence of a planet orbiting one component of the Luhman 16 AB system for masses $\mathcal{M}$ M ≥ 1.5 M♆ (Neptune masses) and periods between 400 and 5000 days. However, the presence of third bodies with masses $\mathcal{M}$ M ≤ M♆ and periods between 2 and 400 days (~ 1.1 years) cannot be excluded. Our measurements make significant improvements to the characterization of this sub-stellar binary, including its mass-ratio 0.8305 ±0.0006, individual component masses 35.4± 0.2 M♃ and 29.4± 0.2 M♃ (Jupiter masses), and parallax distance 1.9960 pc ± 50 AU. Comparison of the masses and luminosities of Luhman 16 AB to several evolutionary models shows persistent discrepancies in the ages of the two components, but strengthens the case that this system is a member of the 510± 95 Myr Oceanus Moving Group.

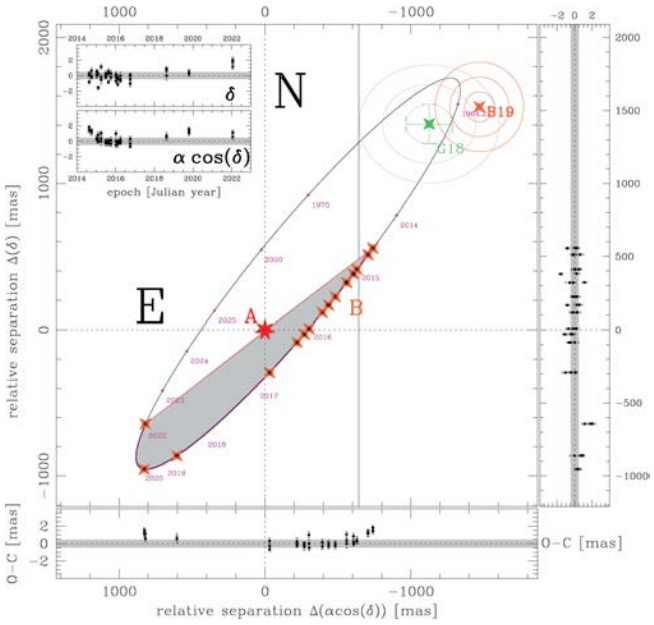


**Figure 4.** The relative orbit of Luhman 16 B (four-pointed star symbols) around A (seven-pointed star symbol at origin). To better highlight the amount of curvature so far observed with HST, a red line connects the first and last observed relative positions, which span approximately 180◦ of orbital phase. For reference, a few epochs are indicated along the orbit in magenta. The lower and right panels show the (O−C) residuals between the relative astrometry and our best-fit orbital model in mas. Grey bands signify the expected uncertainty for any individual relative positional measurement (i.e., √2×0.32 mas). The insets in the large panel show the astrometric residuals in Right Ascension and declination as a function of observing epoch.